




RESEARCH ARTICLE

Intrinsic DNA damage repair deficiency results in progressive microglia loss and replacement

Xiaoming Zhang¹ | Yang Heng¹ | Susanne M. Kooistra¹  |
 Hilmar R. J. van Weering¹ | Maaïke L. Brummer¹ | Emma Gerrits¹ |
 Evelyn M. Wesseling¹ | Nieske Brouwer¹ | Tjalling W. Nijboer¹ |
 Marissa L. Dubbelaar¹ | Erik W. G. M. Boddeke^{1,2}  | Bart J. L. Eggen¹ 

¹Department of Biomedical Sciences of Cells & Systems, Section Molecular Neurobiology, University of Groningen, University Medical Center Groningen, Groningen, The Netherlands

²Center for Healthy Ageing, Department of Cellular and Molecular Medicine, University of Copenhagen, Copenhagen, Denmark

Correspondence

Bart J. L. Eggen, Department of Biomedical Sciences of Cells & Systems, Section Molecular Neurobiology, University of Groningen, University Medical Center Groningen, Antonius Deusinglaan 1, 9713 AV Groningen, The Netherlands.
 Email: b.j.l.eggen@umcg.nl

Funding information

China Scholarship Council fellowships

Abstract

The DNA excision repair protein *Ercc1* is important for nucleotide excision, double strand DNA break, and interstrand DNA crosslink repair. In constitutive *Ercc1*-knockout mice, microglia display increased phagocytosis, proliferation and an enhanced responsiveness to lipopolysaccharide (LPS)-induced peripheral inflammation. However, the intrinsic effects of *Ercc1*-deficiency on microglia are unclear. In this study, *Ercc1* was specifically deleted from Cx3cr1-expressing cells and changes in microglia morphology and immune responses at different times after deletion were determined. Microglia numbers were reduced with approximately 50% at 2–12 months after *Ercc1* deletion. Larger and more ramified microglia were observed following *Ercc1* deletion both in vivo and in organotypic hippocampal slice cultures. *Ercc1*-deficient microglia were progressively lost, and during this period, microglia proliferation was transiently increased. *Ercc1*-deficient microglia were gradually replaced by nondeficient microglia carrying a functional *Ercc1* allele. In contrast to constitutive *Ercc1*-deficient mice, microglia-specific deletion of *Ercc1* did not induce microglia activation or increase their responsiveness to a systemic LPS challenge. Gene expression analysis suggested that *Ercc1* deletion in microglia induced a transient aging signature, which was different from a priming or disease-associated microglia gene expression profile.

KEYWORDS

aging, DNA damage repair, *Ercc1*, microglia, morphometrics

1 | INTRODUCTION

Organisms have developed intricate mechanisms to repair different forms of DNA damage, for example, base excision repair (BER),

nucleotide excision repair (NER), mismatch repair (MMR), inter-strand crosslink repair (ICR), and double-strand break repair (DBR). Repair of DNA damage is important as persistent damage induces cell senescence or cell death (Rodier et al., 2009). Deficiencies in

Xiaoming Zhang and Yang Heng co-first authors.

This is an open access article under the terms of the Creative Commons Attribution-NonCommercial License, which permits use, distribution and reproduction in any medium, provided the original work is properly cited and is not used for commercial purposes.

© 2020 The Authors. GLIA published by Wiley Periodicals LLC



DNA repair pathways lead to various progeria syndromes both in human and mouse (Schumacher, Garinis, & Hoeijmakers, 2008). In many progeria syndromes, neurologic defects occur, which highlights the vital role of genome stability maintenance for the central nervous system (CNS; Heng, Eggen, Boddeke, & Kooistra, 2017; McKinnon, 2013).

Excision repair cross-complementation group 1 (ERCC1) in complex with XPF is an essential nuclease in the NER, ICR and DBR pathways (Ahmad et al., 2008; Klein Douwel et al., 2014; Li et al., 2019). Besides their role in DNA damage repair, nucleotide excision repair factors like ERCC1 and XPF are recruited to active promoters to facilitate transcription (Le May et al., 2010). Mutations in *ERCC1* and *XPF* cause cerebro-oculo-facioskeletal (COFS) syndrome, Cockayne syndrome (CS), and xeroderma pigmentosum (XP) in humans (Gregg, Robinson, & Niedernhofer, 2011; Kashiwama et al., 2013). Mice carrying a knockout (ko) and a hypomorphic (Δ) allele for *Ercc1* (*Ercc1 Δ /ko*) display a range of progeroid changes, including reduced lifespan, loss of the body weight, and various aging-related pathological changes in peripheral organs (Dolle et al., 2011). In addition, constitutive *Ercc1*-knockout (*Ercc1 Δ /ko*) mice display premature CNS aging, such as motor abnormalities and cognitive decline, widespread astrogliosis, microgliosis and neuronal degeneration in the brain, and progressive motor neuron loss in the spinal cord (Borgesius et al., 2011; de Waard et al., 2010; Vegh et al., 2012). Microglia in *Ercc1 Δ /ko* mice exhibit a hypertrophic morphology with thickened primary processes and an increase in soma size (Raj et al., 2014). Functionally, microglia in *Ercc1 Δ /ko* mice show increased phagocytosis, proliferation and reactive oxygen species (ROS) production. Notably, microglia in *Ercc1 Δ /ko* mice are primed (Cunningham, 2013), indicated by an enhanced proinflammatory response to a systemic peripheral inflammatory challenge (intraperitoneal lipopolysaccharide [LPS] injection; Raj et al., 2014). Specific deletion of *Ercc1* in forebrain neurons (*Camk2^{wt/cre}:Ercc1^{ko/loxP}*) showed that neuronal genotoxic stress was sufficient to induce microglia priming (Raj et al., 2014).

We previously reported that a microglia priming gene expression signature is shared between *Ercc1 Δ /ko* mice, Alzheimer's disease (AD), and amyotrophic lateral sclerosis (ALS) mouse models and naturally aged mice (Holtman et al., 2015). This profile is characterized by the upregulation of genes associated with immune, phagosome, and antigen presentation pathways and the downregulation of homeostatic microglia genes (Holtman et al., 2015). Similarly, microglia in CNS disease mouse models exhibit increased phagocytic and immune activity and are referred to as disease-associated microglia (DAM) or microglia in neurodegenerative disease (MGnD; Butovsky & Weiner, 2018; Keren-Shaul et al., 2017; Krasemann et al., 2017; Mathys et al., 2017). Where constitutive *Ercc1* deletion induces microglia priming, the effect of microglia-specific *Ercc1*-deficiency is unclear. In this study, the *Ercc1* gene was deleted from microglia and the effect on microglia density, morphology, survival, proliferation, and responsiveness to LPS-induced inflammation were determined.

2 | MATERIALS AND METHODS

2.1 | Animals

Cx3cr1^{wt/creERT2} (JAX stock #021160), *Ercc1^{wt/ko}* and *Ercc1^{loxP/loxP}* mouse lines were crossed to obtain the experimental lines *Cx3cr1^{wt/creERT2}:Ercc1^{ko/loxP}* and *Cx3cr1^{wt/creERT2}:Ercc1^{wt/loxP}* (Figure S1a). In brief, *Cx3cr1^{wt/creERT2}:Ercc1^{wt/ko}* mice were generated by crossing *Ercc1^{wt/ko}* and *Cx3cr1^{wt/creERT2}* mice (both in a C57BL/6 background). *Cx3cr1^{creERT2/creERT2}:Ercc1^{wt/ko}* were crossed with *Ercc1^{loxP/loxP}* mice (FVB background), resulting in *Cx3cr1^{wt/creERT2}:Ercc1^{ko/loxP}* and *Cx3cr1^{wt/creERT2}:Ercc1^{wt/loxP}* mice (Figure S1a, hereafter referred to as *Cx3cr1-Ercc1^{ko/loxP}* and *Cx3cr1-Ercc1^{wt/loxP}* mice). The mice were group-housed with 2–4 same-sex littermates per cage under 12-hour light/dark cycle conditions and ad libitum access to food and water. All experiments were performed in the Central Animal Facility (CDP) of the UMCG, with protocol (15360-03-002) approved by the Animal Care and Use Committee of the University of Groningen.

2.2 | Genotyping

Genomic DNA was isolated from ear cuts for genotyping with MyTaq Extract-PCR Kit (Bioline, BIO-21127). Primer information is provided in Table S1. *Cx3cr1-cre* was genotyped by PCR with *cre* primers (Table S1). Schematic representation of *Ercc1^{wt}*, *Ercc1^{ko}*, *Ercc1^{loxP}*, and recombined *Ercc1^{rec}* alleles are depicted in Figure S1b. The *Ercc1^{ko}* allele consisted of a *neo* cassette insertion interrupting Exon 7, aborting the essential carboxy-terminal 74 amino acids of *Ercc1* (Weeda et al., 1997). In the *Ercc1^{loxP}* allele, Exons 3–5 are flanked by loxP sites (Doig et al., 2006). After tamoxifen treatment, Exons 3–5 in the *Ercc1^{loxP}* allele will be deleted by homologous recombination, resulting in a recombined *Ercc1^{rec}* allele. In *Ercc1^{wt/ko}* and *Cx3cr1-Ercc1^{wt/ko}* mouse line, genotyping of the *Ercc1^{wt}* and *Ercc1^{ko}* was done by duplex PCR using *wt* and *neo* primer pairs (Table S1) as described before (Ahmad et al., 2008). For *Cx3cr1-Ercc1^{ko/loxP}* and *Cx3cr1-Ercc1^{wt/loxP}* mouse lines, a duplex PCR was performed to distinguish *Ercc1^{wt}*, *Ercc1^{ko}*, and *Ercc1^{loxP}* alleles using *loxP* and *neo* primer pairs (Table S1).

After tamoxifen treatment, the *Ercc1^{loxP}* alleles in both *Cx3cr1-Ercc1^{wt/loxP}* and *Cx3cr1-Ercc1^{ko/loxP}* mice microglia are recombined (*Ercc1^{rec}*) (Figure S1c). This recombination results in full *Ercc1* deletion in *Cx3cr1-Ercc1^{ko/loxP}* mice microglia, but only partial deletion in *Cx3cr1-Ercc1^{wt/loxP}* mice microglia, since one *Ercc1^{wt}* allele is still present (Figure S1c). To confirm the specific deletion of *Ercc1* in microglia, all mice were genotyped by genomic PCR on sorted microglia (Figure S1d). Mice of 6–8 weeks of age received tamoxifen to induce *Ercc1* gene recombination. At certain time points post tamoxifen treatment, microglia were FACS-sorted and DNA was isolated from these microglia for genotyping. A duplex PCR was performed to distinguish *Ercc1^{wt}*, *Ercc1^{ko}*, and *Ercc1^{loxP}* allele using *loxP* and *neo* primer pairs (Table S1), and *Ercc1^{rec}* was genotyped using *rec*

primer pair (Table S1). The *Ercc1*^{wt} (~1,000 bp), *Ercc1*^{ko} (~800 bp), and *Ercc1*^{loxP} (~500 bp) products were separated by electrophoresis on 1.2% agarose gels, and the *Ercc1*^{rec} allele generated a ~280 bp PCR product (Figure S1d).

2.3 | Administration of tamoxifen

Mice of 6–8 weeks of age received 2 doses of 500 µl of tamoxifen (20 mg/ml, Sigma-Aldrich, T5648) dissolved in corn oil (Sigma-Aldrich, C8267) via oral gavage with a 48 hr interval as described previously (Parkhurst et al., 2013).

2.4 | LPS treatment

Mice were given an intraperitoneal (i.p.) injection of 1 mg/kg LPS (Sigma-Aldrich, *Escherichia coli* O11:B4, L4391) dissolved in Dulbecco's phosphate buffered saline (DPBS, Lonza, BE17512F). Control mice received a respective volume of DPBS. After 3 hr, animals were perfused with saline or PBS under deep anesthesia and the brains were collected.

2.5 | Microglia isolation and flow cytometry

Microglia were isolated as described in our previous work (Gerrits, Heng, Boddeke, & Eggen, 2020). Mice were perfused with saline or PBS under deep anesthesia. Brains were placed in Hank's balanced salt solution (HBSS, Gibco, 14170-088) with 0.6% glucose (Sigma-Aldrich, G8769) and 15 mM HEPES (Lonza, BE17-737E). All the following isolation procedures were performed on ice or at 4°C during centrifugation. Brains were mechanical dissociated using the Potter-Elvehjem tissue homogenizer and centrifuged at 220g for 10 min. The pellets were resuspended in 25 ml 24% Percoll (GE Healthcare, 17-0891-01) with a 3 ml PBS layer on top, followed by centrifugation for 20 min at 950g (accelerate 4 and brake 0) to remove myelin. The cell pellets were incubated with CD11b-PE (eBioscience, 12-0112-82), CD45-PE/Cy7 (eBioscience, 25-0451-82), and Ly-6C-APC (Biolegend, 128015) antibodies for 20–30 min on ice. Then the cells were washed once and filtered into FACS tubes. Microglia were FACS-sorted as DAPI^{neg}CD11b^{high} CD45^{int} Ly6c^{neg} events on sorter MoFlo-Astrios or MoFlo-XDP (Beckman Coulter).

Ki67 staining was performed according to the manufacturer's protocol. In brief, the cell pellets after the Percoll gradient were permeabilized by adding 1 ml cold 70% ethanol drop by drop while vortexing. After 1 h incubation at –20°C, the cells were twice washed with 1 ml PBS with 10% FBS and incubated with CD11b-PE (eBioscience, 12-0112-82), CD45-FITC (eBioscience, 11-0451-85), Ly-6C-APC/Cy7 (Biolegend, 128025), and Ki67-Alexa Fluor® 647 antibody (Biolegend, 652407) for 30 min. Ki67⁺ microglia and Ki67[–] microglia were collected.

2.6 | Genomic DNA and RNA isolation from microglia

The AllPrep DNA/RNA Micro Kit (Qiagen, 80284) was used to extract genomic DNA and total RNA from sorted microglia.

2.7 | Quantification of recombination efficiency in bulk microglia by quantitative real-time PCR (qPCR)

To investigate recombination efficiency, DNA from microglia from *Cx3cr1-Ercc1*^{ko/loxP} and *Cx3cr1-Ercc1*^{wt/loxP} mice was analyzed by qPCR. Two primer sets were designed, based on the recombined *Ercc1*^{rec} allele: *Ercc1-rec1* and *Ercc1-rec2* (Table S1). Without recombination, the primer sets will not give products during the PCR due to the long span between the forward and reverse primer. In addition, a reference primer pair, *Ref-Il1*, which amplifies a genomic fragment of the *Il1* gene was included (Table S1). The PCR reaction mixture contained 5 µl DNA template from microglia samples, 5.5 µl iTaq™ Universal SYBR® Green Supermix (Bio-Rad, 1725125), 0.3 µl ddH₂O and 0.2 µl 10 µM primer mix. Each sample was quantified with three technical replicates. The percentage of microglia with a recombinant *Ercc1*^{rec} allele was calculated by the following formula (Livak & Schmittgen, 2001).

$$\begin{aligned} \text{Percentage of microglia with } Ercc1^{rec} \text{ allele} &= \\ & \frac{\text{microglia } (Ercc1^{rec})}{\text{microglia } (Ercc1^{rec}) + \text{microglia } (Ercc1^{loxP})} \\ &= 2^{-\left(\frac{Ct(Ercc1-rec1) + Ct(Ercc1-rec2)}{2} - Ct(Ref-Il1) - 1\right)} \end{aligned}$$

2.8 | Quantification of recombination efficiency by single-cell qPCR (genomic DNA)

Individual microglia were FACS-sorted in 384-well PCR plates containing 5 µl ddH₂O in each well. The presence of the *Ercc1*^{rec} allele was determined using qPCR primer pair *Ercc1-rec1*. As a positive control, individual microglia were analyzed using *Ref-Il1* primers. As negative controls, individual splenic macrophage (DAPI^{neg} CD11b^{high}CD45^{pos}Ly6g^{neg}) were sorted in 384 well plates and analyzed. 5.5 µl of iTaq™ Universal SYBR® Green Supermix, 0.3 µl ddH₂O and 0.2 µl 10 µM primer mix were added to each well. Quantitative PCR reactions were performed using the QuantStudio 7 Real-Time PCR system (Thermo Scientific). In the end, the number of PCR reactions resulting in specific DNA products from *Ercc1*^{rec} (with correct melting curves) were quantified. The percentage of microglia with recombinant *Ercc1*^{rec} allele was calculated by the following formula.

$$\begin{aligned} \text{Percentage of microglia with } Ercc1^{rec} &= \\ & \frac{\text{number of PCR reactions with products from } Ercc1^{rec} \text{ allele}}{\text{total number of PCR reactions}} \end{aligned}$$



2.9 | cDNA synthesis and qPCR

RNA isolated from microglia was mixed with 1 μ l random primers (0.5 μ g/ μ l, Invitrogen, 48190011) and ddH₂O to 10 μ l. Samples were incubated at 65°C for 15 min and kept on ice. Thereafter, 8 U/ μ l M-MuLV reverse transcriptase (Thermo Scientific, EP0442), 0.8 U/ μ l Ribolock RNase inhibitor (Thermo Scientific, E00382), 0.5 mM dNTP-mix (Thermo Scientific, R0192) and reverse transcriptase buffer were added and incubated on a thermal cycler at 42°C for 1 hr, at 70°C for 10 min and finally at 4°C. The resulting cDNA was used for qPCR reactions. The PCR reaction mixture contained 5 μ l cDNA template from microglia samples, 5.5 μ l iTaq™ Universal SYBR® Green Super-mix, 0.3 μ l ddH₂O and 0.2 μ l 10 μ M primer mix. Each sample was run with three technical replicates. Quantitative PCR reactions were performed using the ABI7900HT Fast Real-Time PCR System (Thermo Scientific), LightCycler® 480 System (Roche) or QuantStudio 7 Real-Time PCR system (Thermo Scientific). To determine relative expression levels, *Hprt1* was used as the reference gene. Primer sequences are provided in Table S2.

2.10 | QuantSeq 3' mRNA-Sequencing and bioinformatic analysis

RNA quantity and quality were analyzed on a Fragment Analyzer (Agilent), only RNA samples with a RIN value >6.5 were used. Sequencing libraries were prepared with the QuantSeq 3' mRNA-Seq Library Prep Kit FWD (Lexogen, 015.96). Quality control of the raw FASTQ files was performed with FASTQC. Bad quality bases were trimmed with FASTX_trimmer of the FASTX_toolkit (version 0.013). Sequences were aligned using default parameters on HiSAT2 version 2.1 to the *M. musculus* (GRCm38.85) reference template obtained from Ensembl. Quantification of the reads was performed with HTseq-counts (version 0.6.1). Raw count matrices were loaded in R and processed with DESeq2. Genes were identified as differentially expressed with an FDR < 0.05 and fold change >1.5. Normalized values (counts per million) of the differentially expressed genes were used as heatmap input. Gene ontology (GO) term enrichment analysis was performed using Metascape (<http://www.metascape.org/>).

2.11 | Immunohistochemistry and immunofluorescence

To collect brain tissue for immunostaining, mice were perfused with saline under deep anesthesia. Brains were fixed for 48 hr in 4% paraformaldehyde (PFA) at 4°C. After dehydration in 25% sucrose, the brain samples were embedded with O.C.T. compound (Sakura Finetek, 4583) and stored at -80°C.

For immunohistochemistry, 16 μ m sections were prepared by cryo-sectioning. After washing thrice with 1 \times PBS (identical for all subsequent washing steps), antigen retrieval was performed by

pressure cooking in 10 mM sodium citrate, pH 6.0. The sections were washed and incubated in PBS with 1% hydrogen peroxide (H₂O₂) to block endogenous peroxidases. Again, the sections were washed and blocked for 30 min using 5% normal donkey serum (NDS; Jackson Immuno Research, 017-000-121) in PBS with 0.3% Triton X-100 (PBS⁺). Afterward, the sections were incubated with the primary rabbit- α -ionized calcium-binding adapter molecule 1 (Iba1) antibody (1:1,000; Wako, 01-19741) overnight at 4°C. The following day, the slides were washed and incubated with the biotinylated secondary donkey- α -rabbit IgG antibody (1:400; Jackson Immuno Research, 711-065-152) for 1 hr. After washing, the sections were incubated with ABC solution (VECTASTAIN® ABC Kit, Vector Laboratories, PK-6100) for 30 min. The sections were washed, stained using 0.04% 3,3'-Diaminobenzidine (DAB) and 0.01% H₂O₂ for 8 min and subsequently dehydrated using a sequence of increasing ethanol concentrations. The slides were air dried for 30 min, mounted with coverslips using DePex (Serva) and stored at room temperature. All the slides were scanned with the NanoZoomer 2.0-HT Digital Pathology system (Hamamatsu Photonics, K.K., Japan) at 40 times magnification.

For immunofluorescence, free-floating brain sections were immunolabeled as described (Sierra et al., 2010). For organotypic hippocampal slice culture, slices were blocked for 1 hr with 5% normal donkey serum and thereafter incubated with a primary antibody against Iba1 (1:1,000; Wako, 019-19741) overnight at 4°C. On the next day, after washing thrice with 1 \times PBS, Alexa Fluor 488 donkey anti-rabbit (1:400; Invitrogen, A21206) secondary antibody was added. After 1 hr of secondary antibody incubation, sections were washed and incubated in Hoechst solution (1 μ g/ml, Sigma-Aldrich, 14530) for 5 min. After washing, the slides were mounted with Mowiol mounting medium on glass slides. Image acquisition was performed using a Leica SP8 confocal microscope system (TCS SP8, Leica Microsystems).

2.12 | Microglia density and spatial distribution analysis

Microglia densities in the frontal cortex and in *cornu ammonis* (CA), and *dentate gyrus* (DG) were determined by counting all Iba1-positive cells in a specified region of interest (ROI) of known dimensions using the cell counter plugin for the ImageJ software (<http://rsb.info.nih.gov/ij/>). To assess the spatial distribution of microglia in the frontal cortex, the nearest neighbor distances—that is, the average Euclidian distances between nearest cells—were determined using the NND plugin for ImageJ. 2–3 ROIs were selected per animal per group for the analysis. Three mice per group were used except the 22 months ($n = 2$).

2.13 | Morphometric analysis of microglia

A pipeline was developed to analyze morphological changes in microglia (Van Weering et al., in prep.). Briefly, single-cell images of

iba1-positive cells were first extracted from the whole slide scans, with at least 20 cells per region per animal. Prior to analysis, the single cell images were preprocessed to cell silhouette images by semi-automated thresholding. Subsequently, the cell silhouettes were converted to cell skeleton images by repeated thinning and pruning of the branch areas. In the cell skeleton, branch endings (end nodes), branch crossings (junctions), and all branch points emanating from the cell soma (start nodes) were tagged to allow node quantification. Both cell silhouette- and cell skeleton images served as input for fully automated morphometric analysis. The outputs of the pipeline included Sholl analysis result and morphometric features per cell. A specified list of morphometric features, as well as a detailed description of the morphometrics pipeline is described elsewhere (van Weering et al., in prep.).

2.14 | Clustering of microglia based on morphometric features

To identify groups of microglia of similar morphology, a nonsupervised clustering approach was applied (described in detail in van Weering et al., in prep.). In brief, after normalization and scaling of all morphometric features, a principal component analysis (PCA) was applied to reduce dimensionality and redundancy in the dataset. Subsequently, a hierarchical clustering (Ward's method) was performed on the top contributing principal components (PCs) with an eigenvalue >1 (here, PC1–4, Figure S2a), resulting in nine clusters of microglia with distinct morphological properties (Figure S2b). The morphometric properties of each cluster are depicted in Figure S2d.

2.15 | Organotypic hippocampal slice culture

Organotypic hippocampal slice culture (OHSCs) were prepared as described previously (Stoppini et al., 1991) with minor modifications. In brief, brains were rapidly isolated from *Cx3cr1-Erc1^{ko/loxP}* and *Cx3cr1-Erc1^{wt/loxP}* mouse pups (p3) after decapitation. The hippocampi from both hemispheres were isolated in ice cold serum-free HBSS supplemented with 0.5% glucose and 15 mM HEPES. Isolated hippocampi were cut into 375 μ m thick slices using a tissue chopper (Mcllwain) and were transferred to 0.4 μ m culture plate inserts (Millipore, PICM03050). These culture plate inserts, containing 6 slice cultures each, were placed in 6-well plates containing 1.2 ml of culture medium per well. Culture medium (pH 7.2) consisted of 50% minimum essential medium supplemented with 25% heat-inactivated horse serum (Gibco, 16050-122), 25% basal medium eagle, 2 mM glutamax and 0.65% glucose. The slice cultures were kept at 35°C in a humidified atmosphere (5% CO₂). On the first day after preparation, OHSCs were treated with 1 nM 4-hydroxy tamoxifen (Sigma-Aldrich, T176) for 48 hr to induce *Erc1* deletion. OHSCs were kept for up to 3 months and the culture medium was refreshed every 2 days. After fixation with 4% PFA overnight at 4°C, OHSCs were processed for immunofluorescence staining.

2.16 | Quantification and statistical analysis

Statistical significance was determined by either a two-way ANOVA followed by Bonferroni correction or a two-tailed Student's *t*-test as indicated in the legends. For the morphometrics data, after hierarchical clustering, a Kruskal–Wallis test followed by a Wilcoxon rank sum test with Bonferroni correction was performed for comparison of morphometric features between microglia clusters. Statistical differences with *p* values lower than 0.05 were considered significant.

3 | RESULTS

3.1 | Microglia are progressively lost after *Erc1* deletion

Erc1 is an essential endonuclease component in NER, ICR, and DBR, and microglia will accumulate DNA lesions after *Erc1* deletion. Cell cycle arrest, DNA repair, and apoptosis are the general responses to DNA damage (Norbury & Zhivotovsky, 2004). To obtain conditional *Erc1*-deficient mice, *Erc1^{wt/ko}* and *Cx3cr1^{wt/creERT2}* mice were crossed to generate *Cx3cr1^{wt/creERT2}:Erc1^{wt/ko}* mice (Figure S1a). Then, *Cx3cr1^{creERT2/creERT2}:Erc1^{wt/ko}* were crossed with *Erc1^{loxP/loxP}* mice, resulting in *Cx3cr1-Erc1^{ko/loxP}*, and *Cx3cr1-Erc1^{wt/loxP}* mice (Figure S1a). After tamoxifen-induced nuclear translocation of CreER, the *Erc1^{loxP}* alleles in both *Cx3cr1-Erc1^{wt/loxP}* and *Cx3cr1-Erc1^{ko/loxP}* mice microglia were recombined (*Erc1^{rec}*) (Figure S1b,c). This recombination resulted in *Erc1* deficiency in *Cx3cr1-Erc1^{ko/loxP}* mice microglia, but not in *Cx3cr1-Erc1^{wt/loxP}* mice microglia, since one *Erc1^{wt}* allele was still present (Figure S1b,c).

To determine the effect of *Erc1* deletion on microglia, first, the effect on microglia cell density was determined in the frontal cortex (Figure 1a). From 2 months after tamoxifen treatment onward, the density of microglia in the frontal cortex of *Cx3cr1-Erc1^{ko/loxP}* mice was significantly lower than in littermate controls, and this reduction persisted until 12 months after tamoxifen treatment (Figure 1b). A reduction in microglia density after *Erc1* deletion was also observed in other brain regions. In the DG and CA, a significant reduction was observed at 6 and 12 months after tamoxifen treatment (Figure 1b). At 22 months after tamoxifen treatment, microglia density in *Cx3cr1-Erc1^{ko/loxP}* mice was similar to control littermates in all brain regions investigated (Figure 1b). Together with the reduction in microglia density, a significant increase was observed in the nearest neighbor distance between microglia in the frontal cortex of *Cx3cr1-Erc1^{ko/loxP}* mice, suggesting that the observed microglia loss occurred throughout the brain and was not regional (Figure 1c). Similar to our histological data, the number of FACS-sorted microglia from *Cx3cr1-Erc1^{ko/loxP}* mice was significantly lower than from littermate controls. This reduction in the number of isolated microglia persisted from 2 to 12 months after tamoxifen treatment (Figure 1d).

In addition, we generated OHSCs from *Cx3cr1-Erc1^{ko/loxP}* pups and deleted *Erc1* by ex vivo 4-hydroxy-tamoxifen treatment. Similar to our in vivo findings, 3 months after tamoxifen treatment,

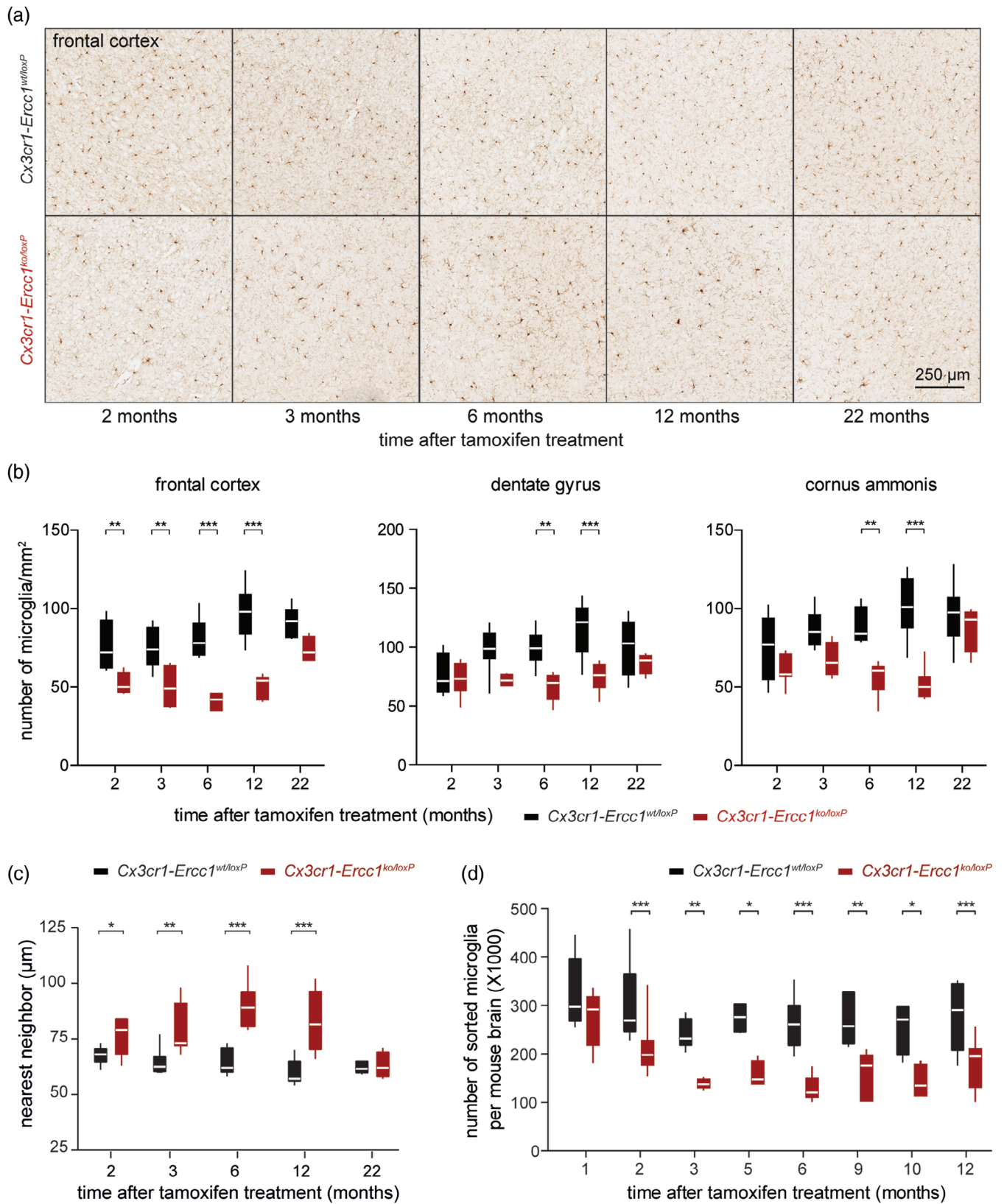


FIGURE 1 Legend on next page.

the number of microglia in *Cx3cr1-Ercc1^{ko/loxP}* OHSCs was reduced by approximately 50% compared to control OHSCs, in the DG, CA1, and CA3 regions (Figure S3a,b).

3.2 | *Ercc1*-deficient microglia are progressively replaced

After tamoxifen treatment, the *Ercc1^{loxP}* allele recombines into an *Ercc1^{rec}* allele in both *Cx3cr1-Ercc1^{ko/loxP}* and *Cx3cr1-Ercc1^{wt/loxP}* mice (Figure S1b,c). To determine the recombination efficiency, genomic DNA was isolated from FACS-isolated microglia and analyzed by qPCR for the *Ercc1^{rec}* allele. In *Cx3cr1-Ercc1^{wt/loxP}* mice microglia, the percentage of microglia with the *Ercc1^{rec}* allele was high (80–100%) and comparable at all investigated time points after tamoxifen treatment (Figure 2a). The percentage of microglia with an *Ercc1^{rec}* allele in *Cx3cr1-Ercc1^{ko/loxP}* mice initially was same as in littermate controls, but progressively declined over time, to approximately 5% at 12 months after tamoxifen treatment (Figure 2a). *Ercc1* recombination efficiency was further determined by single-cell PCR. The percentages of *Ercc1^{rec}* microglia progressively decreased in *Cx3cr1-Ercc1^{ko/loxP}* mice, and very few microglia with an *Ercc1^{rec}* allele were detected at 22 months after tamoxifen treatment (Figure 2b), corroborating our previous observations.

These data indicate that after tamoxifen treatment, *Ercc1*-deficient microglia (*Ercc1^{ko/rec}*) were gradually lost in *Cx3cr1-Ercc1^{ko/loxP}* mice and were replaced by *Ercc1^{ko/loxP}* microglia (Figure 2c). The *Ercc1^{ko/loxP}* microglia are likely cells that escaped tamoxifen induced *Ercc1* deletion, and still carried a functional *Ercc1^{loxP}* allele. At 12 months after tamoxifen treatment, *Ercc1*-deficient microglia were almost completely replaced by *Ercc1^{ko/loxP}* microglia, but microglia numbers were still reduced by approximately 40–50% (Figures 1 and 2). At 22 months after tamoxifen treatment, *Ercc1*-deficient microglia were fully replaced and no differences in microglia densities were observed between control and *Cx3cr1-Ercc1^{ko/loxP}* mice (Figures 1 and 2).

3.3 | Altered microglia morphology in *Cx3cr1-Ercc1^{ko/loxP}* mice

An evident change in microglia morphology was observed in the frontal cortex of *Cx3cr1-Ercc1^{ko/loxP}* mice from 2 to 12 months after

tamoxifen treatment when compared to littermate controls (Figure 3a). Some of the microglia became enlarged, with increased soma sizes and branch lengths (Figure 3a). This altered microglia morphology was also observed in other brain regions, including cortex, hippocampus, cerebellum and olfactory bulb (data not shown). Strikingly, at 22 months after tamoxifen treatment, all microglia in the *Cx3cr1-Ercc1^{ko/loxP}* mice displayed a morphology that was comparable to littermate controls (Figure 3a). In OHSCs, a similar change in microglia morphology was observed in *Cx3cr1-Ercc1^{ko/loxP}* mice (Figure S3c). Next, morphological differences in microglia were quantified across groups at different time points after tamoxifen treatment. The generated 23 morphometric features of each microglia cell are provided in Table S3.

To identify subsets of microglia with a similar morphology, we performed hierarchical clustering on principal components. First, a PCA was applied to the morphometric feature dataset. The first four PCs with an eigenvalue >1 were retained for hierarchical clustering (Figure S2a,b), resulting in 9 microglia clusters with distinct morphological properties (Figure 3b). Cell silhouettes representative for each cluster are depicted in Figure 3c. Notably, microglia in cluster I and II were almost exclusively derived from *Cx3cr1-Ercc1^{ko/loxP}* mice, indicating these microglia clusters are *Ercc1*-deficiency related (Figure 3b). Cluster I and II microglia were characterized by a relatively large soma area, high total branch length values, a large number of end nodes and relatively low cell solidity values (Figures 3c and S2). These findings were corroborated by Sholl analysis with cluster I and II microglia being the largest cells with most extensive ramification patterns compared to other clusters (Figure 3d). Comparisons of all morphometric features between microglia clusters can be found in Table S3. Next, we analyzed the relative distribution of the microglia clusters over the different mouse groups (genotype and time after tamoxifen treatment). In control mice, the relative proportion of cluster II and cluster I microglia remained low or even absent at all timepoints in control animals (Figure 3e). In *Cx3cr1-Ercc1^{ko/loxP}* mice, between 2 and 12 months after tamoxifen treatment, cluster I and II microglia accounted for 45–65% of the total population in the cortex (Figure 3e). At 22 months after tamoxifen treatment, the microglia cluster distribution in *Cx3cr1-Ercc1^{ko/loxP}* and *Cx3cr1-Ercc1^{wt/loxP}* mice was comparable and cluster I and II microglia were almost absent (Figure 3e).

To summarize, upon *Ercc1* deletion, CNS microglia numbers were reduced by approximately 50%, which was accompanied by

FIGURE 1 Reduced microglia numbers in *Cx3cr1-Ercc1^{ko/loxP}* mice after tamoxifen treatment. (a) Representative Iba1 staining of microglia in the frontal cortex of *Cx3cr1-Ercc1^{wt/loxP}* and *Cx3cr1-Ercc1^{ko/loxP}* mice at different time points after tamoxifen treatment. (b) Box plots depict the number of Iba1-positive cells/mm² in three different brain regions. Two to three sections per animal were used for density analysis. $n = 3$ mice per group except the 22 months ($n = 2$). The box boundaries represent first and third quartiles and the center lines indicate the median. Whiskers extend from box boundaries to the minimum and maximum values, respectively. (c) Nearest neighbor distance analysis across groups at different time points after tamoxifen treatment. Two to three sections per animal were used for the analysis. $n = 3$ mice per group except the 22 months ($n = 2$). (d) Boxplot depicts the number of microglia (DAPI^{neg}CD11b^{high}CD45^{int}Ly-6C^{neg}) sorted from the entire mouse brain. For *Cx3cr1-Ercc1^{wt/loxP}* mice: $n = 7$ (1 m), 10 (2 m), 6 (3 m), 4 (5 m), 17 (6 m), 6 (9 m), 4 (10 m), 12 (12 m); *Cx3cr1-Ercc1^{ko/loxP}* mice, $n = 10$ (1 m), 13 (2 m), 6 (3 m), 4 (5 m), 15 (6 m), 5 (9 m), 4 (10 m), 13 (12 m). A two-way ANOVA followed by a Bonferroni correction for multiple comparisons was performed to assess significance. *, $p < 0.05$; **, $p < 0.01$; ***, $p < 0.001$

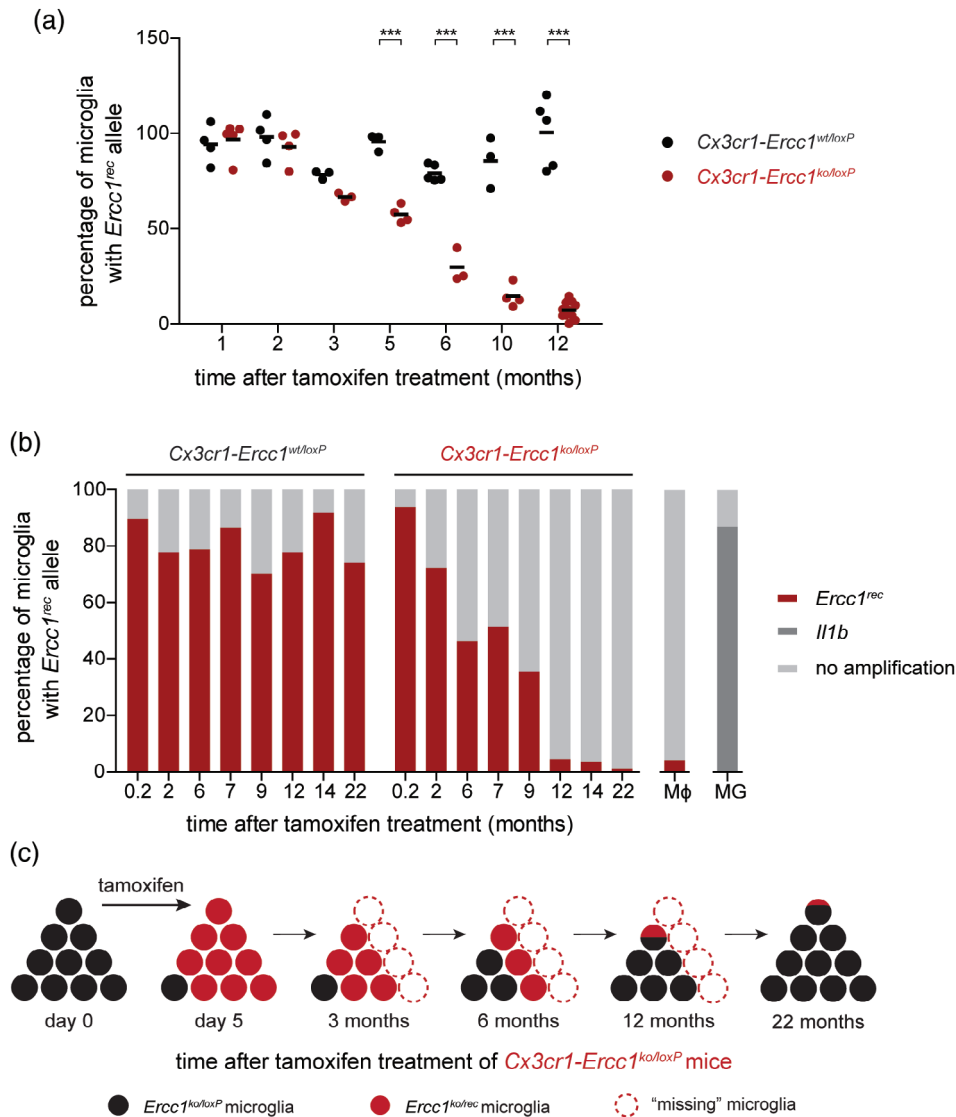


FIGURE 2 *Ercc1*-deficient microglia are gradually replaced by *Ercc1^{ko/loxP}* microglia. (a) The percentage of microglia carrying an excised *Ercc1^{loxP}* allele (*Ercc1^{rec}*) at a range of time points after tamoxifen treatment are depicted. The percentage of microglia with an *Ercc1^{rec}* allele was determined by qPCR using *Ercc1-rec1* and *Ercc1-rec2* primers and normalized to an unaffected genomic locus (the *Il1b* gene). Each dot represents an individual animal. A two-way ANOVA followed by a Bonferroni correction for multiple comparisons was performed to assess significance. ***, $p < 0.001$. (b) The percentage of microglia carrying an *Ercc1^{rec}* allele at a range of time points after tamoxifen treatment was determined by single cell genomic qPCR. Individual microglia were FACS-isolated and PCR amplified using *Ercc1-rec1* primers specific for the *Ercc1^{rec}* allele. The percentage of wells with a PCR product of the *Ercc1^{rec}* allele is shown in red, wells without a PCR product are indicated in light grey. As a positive control, individual microglia (MG) were PCR amplified using primers for the *Il1b* gene, indicated in dark grey. As a negative control, individual splenic macrophages (Mφ) were analyzed with *Ercc1-rec1* primers. $n = 1-3$ animals per group. (c) A cartoon illustrating the progressive loss of microglia cells and the gradual replacement of *Ercc1*-deficient (*Ercc1^{ko/rec}*) microglia by nondeficient (*Ercc1^{ko/loxP}*) microglia in *Cx3cr1-Ercc1^{ko/loxP}* mice after tamoxifen treatment

the emergence of a microglia subpopulation (Cluster I and II) with relatively large and hyper-ramified cells. This reduction in cell number and changes in microglia morphology persisted until 12 months after tamoxifen treatment. Gradually, microglia numbers and morphology returned to control levels at 22 months after tamoxifen treatment.

3.4 | Increased proliferation compensates for microglia loss after *Ercc1* deletion

Under homeostatic conditions, the proliferation rate of microglia is relatively low and the population is maintained by balanced proliferation and apoptosis (Askew et al., 2017). After genetic or

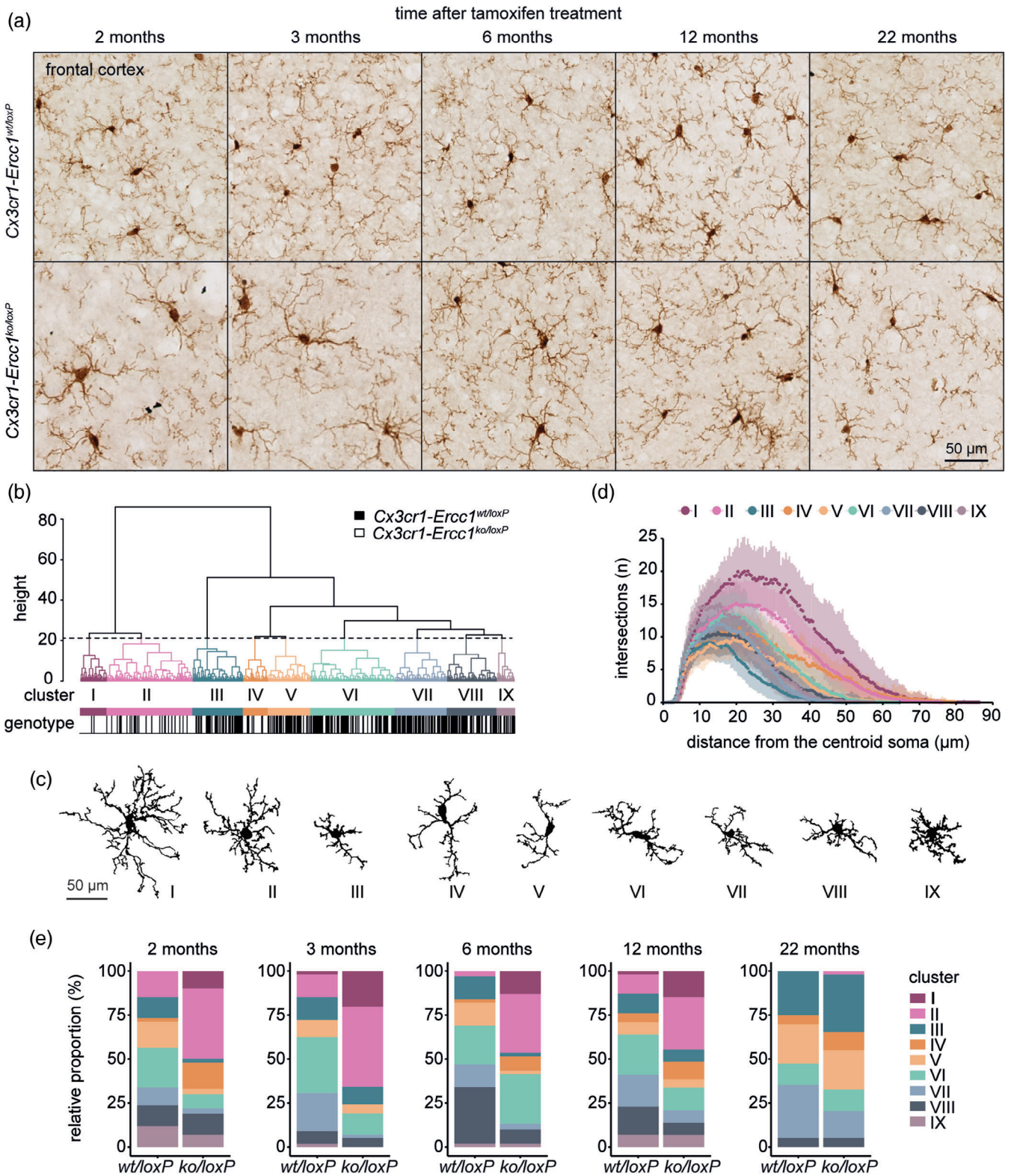


FIGURE 3 Altered microglia morphology in *Cx3cr1-Ercc1*^{ko/loxP} mice. (a) Representative images of Iba1-stained microglia in the cortex of *Cx3cr1-Ercc1*^{wt/loxP} and *Cx3cr1-Ercc1*^{ko/loxP} mice at different time points after tamoxifen treatment. (b) Hierarchical clustering on principal components resulted in nine cell clusters (I–IX). (c) Representative cells for each microglia cluster. (d) Sholl analysis for microglia clusters I–IX, revealing distinct differences in cell size and branching complexity between clusters. Dots and vertical lines represent means and \pm standard deviations respectively. (e) Distribution analysis of microglia clusters across genotypes at different time points after tamoxifen; *wt/loxP*: *Cx3cr1-Ercc1*^{wt/loxP}, *ko/loxP*: *Cx3cr1-Ercc1*^{ko/loxP}

pharmacological depletion of microglia, the remaining microglia rapidly expand and repopulate the CNS (Bruttger et al., 2015; Elmore et al., 2014; Rubino et al., 2018). As *Ercc1*-deficient microglia were gradually replaced, we determined if microglia proliferation was increased after *Ercc1* deletion. The expression levels of *Ki67*, a gene expressed by proliferating microglia (McDonough et al., 2020), was determined in microglia at early (1 and 2 months) and late (12 months)

time points after tamoxifen treatment. Microglia from *Cx3cr1-Ercc1^{ko/loxP}* mice expressed significantly higher *Ki67* levels at 1–2 months after tamoxifen, indicating increased microglia proliferation (Figure 4a). Dividing microglia were observed in the *Cx3cr1-Ercc1^{ko/loxP}* mouse hippocampus 1.5 months after tamoxifen treatment (Figure 4b, indicated by white arrows). At 12 months after tamoxifen, when almost all *Ercc1*-deficient microglia were replaced, *Ki67* expression levels had

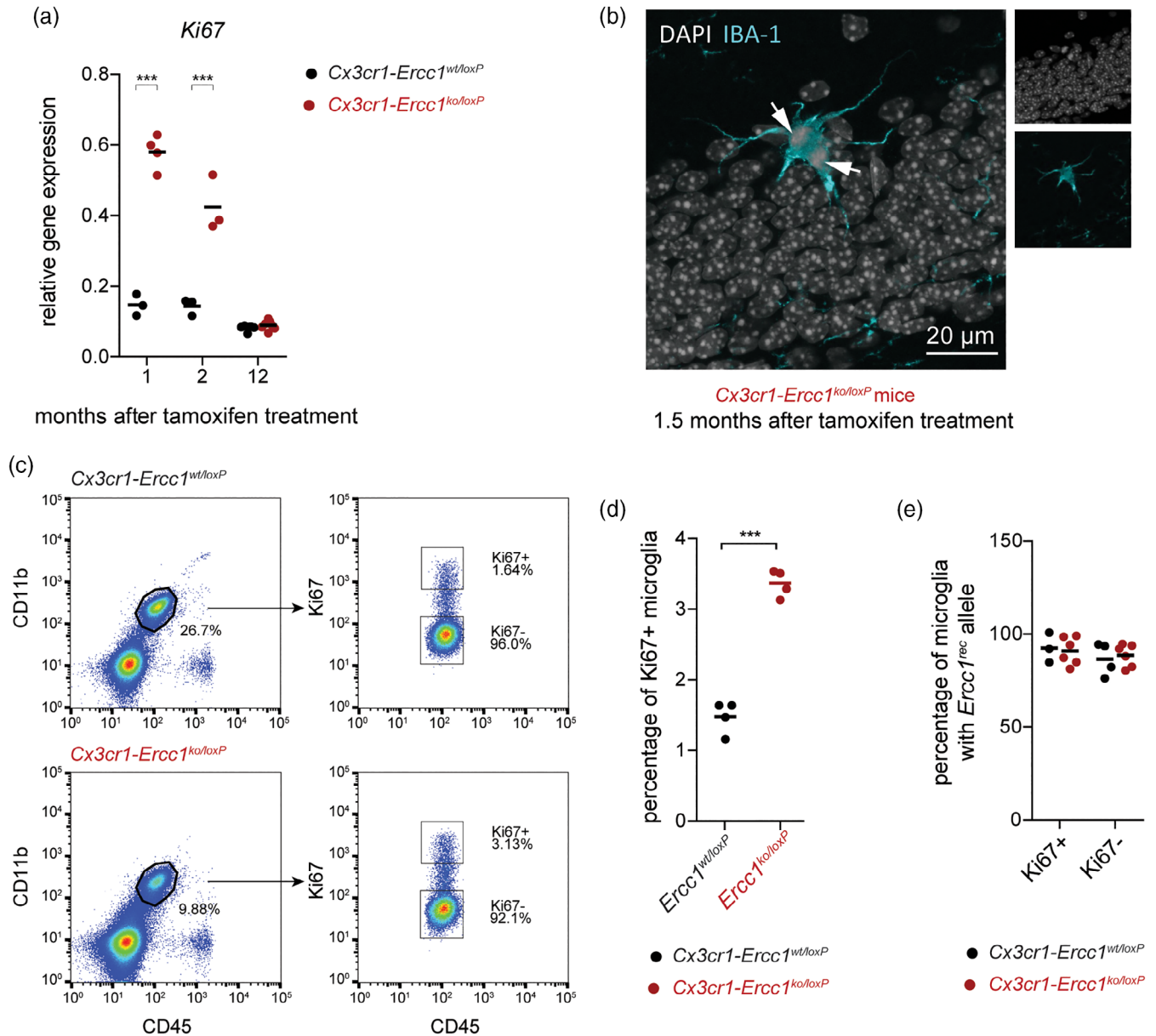


FIGURE 4 Increased microglia proliferation in *Cx3cr1-Ercc1^{ko/loxP}* mice after tamoxifen treatment. (a) *Ki67* gene expression was determined by qPCR and normalized to *Hprt1* expression levels. Each dot represents one animal, $n = 3-5$ mice per group. A two-way ANOVA followed by a Bonferroni correction was performed. $***, p < 0.001$. (b) Example of a mitotic microglia in a *Cx3cr1-Ercc1^{ko/loxP}* mouse, 1.5 months after tamoxifen treatment. (c) FACS plots showing the isolation of *Ki67⁺* and *Ki67⁻* microglia from *Cx3cr1-Ercc1^{wt/loxP}* and *Cx3cr1-Ercc1^{ko/loxP}* mice at 2–3 months after tamoxifen treatment. Percentage of *Ki67⁺* and *Ki67⁻* microglia from *Cx3cr1-Ercc1^{wt/loxP}* and *Cx3cr1-Ercc1^{ko/loxP}* mice was indicated in the plot. (d) Quantification of the percentage of *Ki67⁺* and *Ki67⁻* microglia in *Cx3cr1-Ercc1^{wt/loxP}* and *Cx3cr1-Ercc1^{ko/loxP}* mice at 2–3 months after tamoxifen treatment, $n = 4$ mice per group. An unpaired two-tailed *t*-test was performed. $***, p < 0.001$. (e) The percentage of *Ki67⁺* and *Ki67⁻* microglia with *Ercc1^{rec}* allele was determined by genomic qPCR, $n = 3-6$ mice per group. A two-way ANOVA followed by a Bonferroni correction for multiple comparisons was performed to assess significance

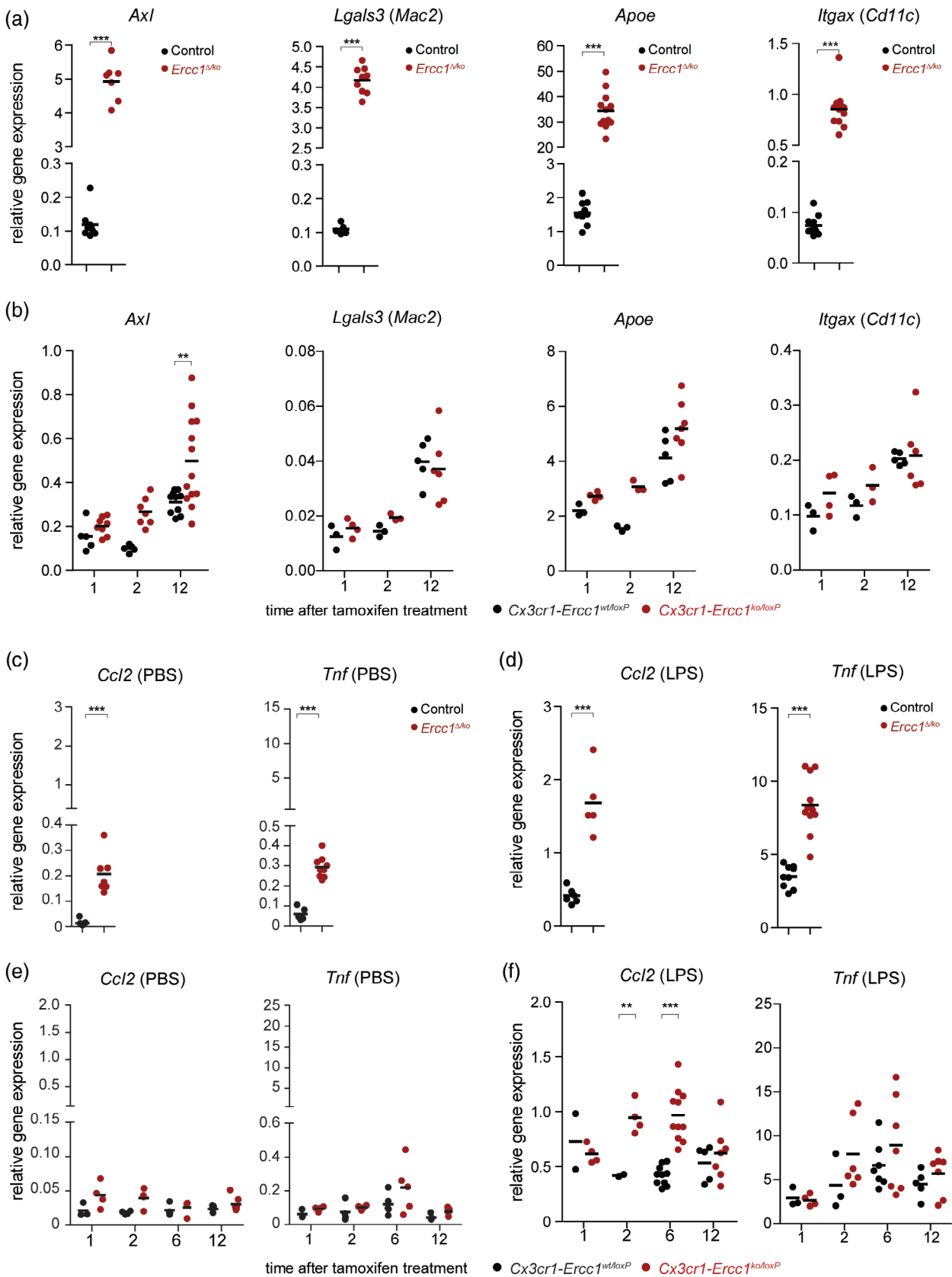


FIGURE 5 Legend on next page.

returned to levels observed in control microglia (Figure 4a). Next, we determined if *Ki67* expressing, proliferating microglia were cells carrying an *Ercc1^{loxP}* allele or if *Ercc1*-deficient microglia also proliferated. Microglia were isolated 2–3 months after tamoxifen treatment when the majority of the cells are still *Ercc1*-deficient (see Figure 2). These microglia were separated in *Ki67⁺* and *Ki67⁻* subpopulations by FACS (Figure 4c). The percentage of *Ki67⁺* cells was more than two-fold higher in microglia from *Cx3cr1-Ercc1^{ko/loxP}* mice compared to *Cx3cr1-Ercc1^{wt/loxP}* controls (Figure 4c,d). Genotyping of *Ki67⁺* microglia population revealed that the percentage of microglia with an *Ercc1^{rec}* allele from both *Cx3cr1-Ercc1^{ko/loxP}* and *Cx3cr1-Ercc1^{wt/loxP}* mice was comparable, indicating that *Ercc1*-deficient microglia (*Ercc1^{ko/rec}*) also proliferated (Figure 4e).

In summary, tamoxifen treatment resulted in *Ercc1* excision, leading to a progressive loss of *Ercc1*-deficient microglia in *Cx3cr1-Ercc1^{ko/loxP}* mice. In parallel, the remaining microglia, including *Ercc1*-deficient microglia, displayed increased expression of proliferation marker *Ki67*. At 12 months after tamoxifen treatment, when nearly all *Ercc1*-deficient microglia (*Ercc1^{ko/rec}*) were replaced by *Ercc1^{ko/loxP}* microglia, *Ki67* expression returned to control levels.

3.5 | *Ercc1*-deficient microglia are not immune activated or primed

In *Ercc1^{Δ/ko}* mouse microglia, the expression of genes like *Axl*, *Lgals3* (*Mac2*), *Apoe*, and *Itgax* (*Cd11c*) is upregulated (Holtman et al., 2015; Figure 5a). The expression of these genes was also determined in *Ercc1*-deficient microglia from *Cx3cr1-Ercc1^{ko/loxP}* mice at different time points after tamoxifen treatment. The expression of *Axl* was significantly higher in *Cx3cr1-Ercc1^{ko/loxP}* microglia only at 12 months compared to *Cx3cr1-Ercc1^{wt/loxP}* microglia, but the level of induction was much lower than in *Ercc1^{Δ/ko}* mice (Figure 5a,b). *Lgals3*, *Apoe*, and *Itgax* expression was not significantly induced in microglia from *Cx3cr1-Ercc1^{ko/loxP}* mice, suggesting microglia were not primed (Figure 5b).

In agreement with our previous findings, basal expression levels of *Ccl2* and *Tnf* were slightly higher in *Ercc1^{Δ/ko}* mice (Figure 5c) and *Ercc1^{Δ/ko}* mice microglia showed an increased responsiveness to LPS compared to controls in terms of *Ccl2* and *Tnf* expression (Raj et al., 2014; Figure 5d). For *Cx3cr1-Ercc1^{ko/loxP}* microglia, basal expression levels of *Ccl2* and *Tnf* were similar to *Cx3cr1-Ercc1^{wt/loxP}* microglia, again suggesting *Cx3cr1-Ercc1^{ko/loxP}* microglia were not

primed (Figure 5e). In response to LPS, *Cx3cr1-Ercc1^{ko/loxP}* microglia only showed a (modest) enhanced *Ccl2* expression at 2 and 6 months after tamoxifen treatment (Figure 5f). For *Tnf* expression, no increase in LPS responsiveness was observed in *Cx3cr1-Ercc1^{ko/loxP}* microglia. (Figure 5f). In summary, microglia-specific deletion of *Ercc1* did not induce an immune activated or primed phenotype in microglia.

3.6 | Gene expression profiling of microglia after *Ercc1* deletion

To delineate the effect of *Ercc1* deletion on microglia, we compared the gene expression profiles between *Cx3cr1-Ercc1^{ko/loxP}* and *Cx3cr1-Ercc1^{wt/loxP}* microglia, before and at different times after tamoxifen treatment (Figures 6a and S4).

Genes in Cluster 1 were more enriched in *Cx3cr1-Ercc1^{wt/loxP}* microglia at 12 months than 5 days after tamoxifen treatment (Figure 6b), suggesting changes in expression of these genes are age-related. Cluster 1 genes were associated with GO terms such as brain development, neuronal system, synapse, and morphogenesis (Figure 6c). Some cluster 1 genes, that showed increased expression in microglia isolated from mice 12 months after tamoxifen (from both genotypes), were also transiently increased in *Cx3cr1-Ercc1^{ko/loxP}* mice microglia at 1 and 2 months after tamoxifen treatment, when most microglia were still *Ercc1*-deficient (Figures 6b and 2). However, with ongoing microglia replacement, around 6 months after tamoxifen treatment. The expression level of these genes was reduced, suggesting *Ercc1* deficiency caused a transient aging phenotype in microglia 1–2 months after tamoxifen treatment (Figure 6b). When microglia were fully replaced in *Cx3cr1-Ercc1^{ko/loxP}* mice at 12 months after tamoxifen treatment (Figure 2), the transcriptional profiles of *Cx3cr1-Ercc1^{ko/loxP}* and *Cx3cr1-Ercc1^{wt/loxP}* mice microglia were again very similar (Figure 6b).

To get more insight into the transient microglia aging phenotype, several homeostatic microglia signature genes, inflammatory genes expressed by potentially senescent human microglia (Geirsdottir et al., 2019), and DAM genes were investigated (Geirsdottir et al., 2019; Keren-Shaul et al., 2017). Expression levels of homeostatic microglia genes, such as *Sall1*, *Cx3cr1*, and *Csf1r* were unaffected by *Ercc1* deletion (Figure S5a). However, at 2 and 6 months after tamoxifen treatment, microglia isolated from *Cx3cr1-Ercc1^{ko/loxP}* mice displayed a transient aging phenotype with higher expression levels of some senescence-associated genes (*Tnf*, *Ccl3* and *Ccl4*) and

FIGURE 5 *Ercc1*-deficient microglia are not immune activated or primed. (a) The expression of *Axl*, *Lgals3*, *Apoe*, and *Itgax* was determined by qPCR in microglia from *Ercc1^{Δ/ko}* mice and normalized to *Hprt1* expression levels. An unpaired two-tailed Student's *t*-test was performed for statistical analysis. ***, $p < 0.001$. (b) *Axl*, *Lgals3*, *Apoe* and *Itgax* gene expression was determined by qPCR in microglia from *Cx3cr1-Ercc1^{wt/loxP}* and *Cx3cr1-Ercc1^{ko/loxP}* mice at different time points after tamoxifen treatment and normalized to *Hprt1* expression levels. A two-way ANOVA followed by a Bonferroni correction for multiple comparisons was performed for statistical analysis. **, $p < 0.01$. Gene expression levels of *Ccl2* and *Tnf* were determined by qPCR in microglia from *Ercc1^{Δ/ko}* and control mice 3 hr after an i.p. PBS (c) or 1 mg/kg LPS (d) and normalized to *Hprt1* expression levels. Each dot represents a mouse. An unpaired two-tailed Student's *t*-test was performed for statistical analysis. ***, $p < 0.001$. Gene expression levels of *Ccl2* and *Tnf* were determined by qPCR in microglia from *Cx3cr1-Ercc1^{wt/loxP}* and *Cx3cr1-Ercc1^{ko/loxP}* mice 3 hr after an i.p. PBS (e) or 1 mg/kg LPS (f) and normalized to *Hprt1* expression levels. Each dot represents a mouse. A two-way ANOVA followed by a Bonferroni correction was performed. **, $p < 0.01$, ***, $p < 0.001$

some of the DAM genes (*ApoE*, *Cst7*, and *Axl*) (Figure S5b,c). But this microglia aging phenotype was no longer detected at 12 months after tamoxifen treatment in *Cx3cr1-Ercc1^{ko/loxP}* mice (Figure S5b,c).

The expression of the majority of the genes in Clusters 2 and 3 was increased at 1 and 2 months after *Ercc1* deletion, and progressively returned to control levels from 6 to 12 months (Figure 6b).

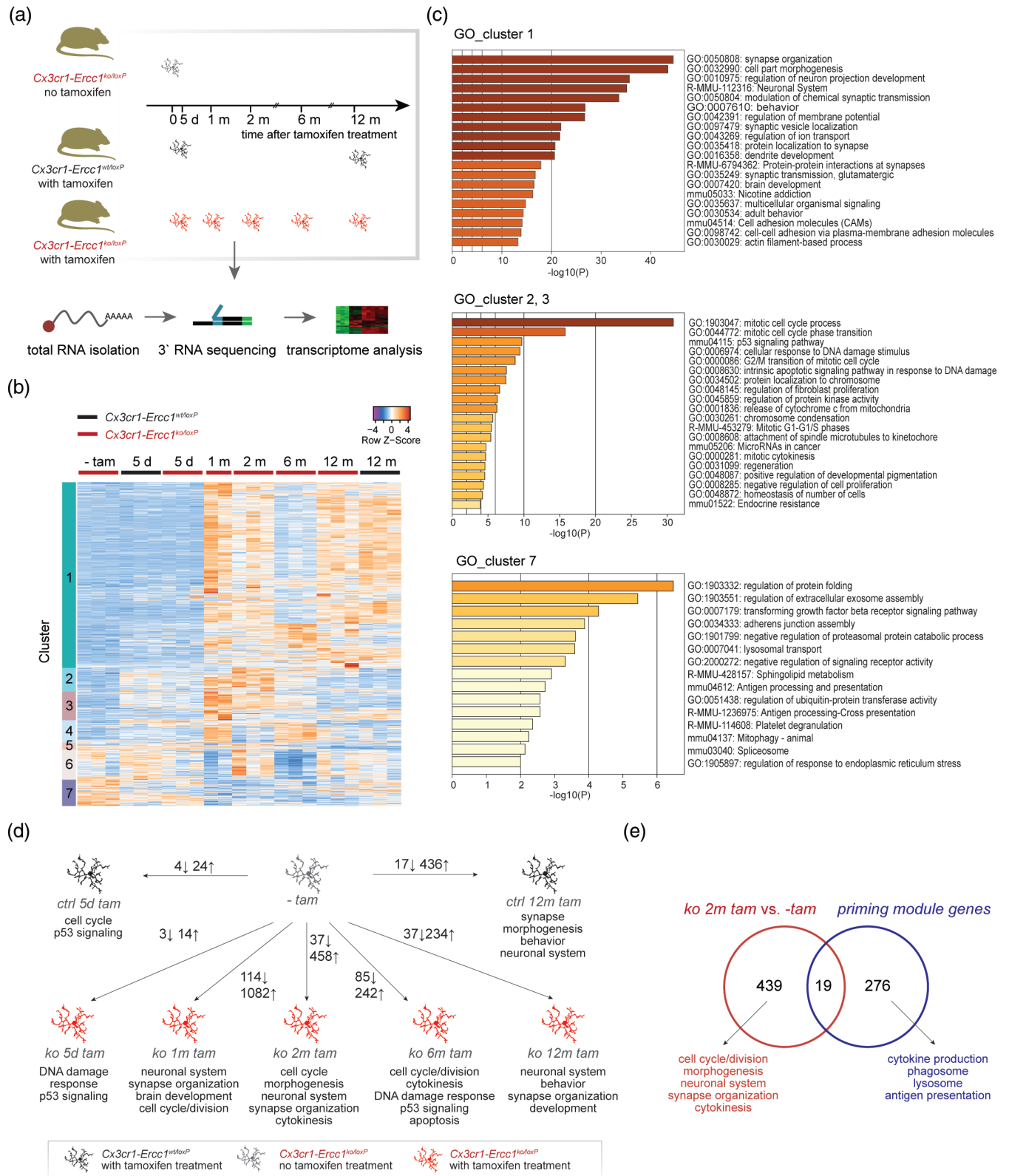


FIGURE 6 Legend on next page.

Some genes in these clusters were associated with mitosis/cell cycle, corroborating the observed increased microglia proliferation at 1 and 2 months after tamoxifen treatment (Figures 6c and 4). In addition, some GO terms of Clusters 2 and 3 genes were related with apoptosis processes such as p53 signaling, release of cytochrome c from mitochondria and intrinsic apoptotic signaling pathway in response to DNA damage (Figure 6c). This supports the excessive loss of *Ercc1*-deficient microglia between 1 and 6 months after tamoxifen treatment (Figure 1).

Cluster 7 contained genes that were downregulated in *Ercc1*-deficient microglia at 1, 2-, and 6-months after tamoxifen treatment. GO enrichment indicated that these genes were involved in regulation of protein folding, extracellular exosome assembly, and lysosomal transport (Figure 6c).

To determine if tamoxifen treatment affected gene expression, the transcriptomes of microglia from *Cx3cr1-Ercc1^{ko/loxP}* mice without tamoxifen treatment and *Cx3cr1-Ercc1^{wt/loxP}* mice 5 days after tamoxifen treatment were compared. We only identified 28 differentially expressed genes which were involved in p53 signaling and cell cycle (Figure 6d), indicating a limited influence of tamoxifen treatment on microglia gene expression. No differentially expressed genes were detected between *Cx3cr1-Ercc1^{wt/loxP}* and *Cx3cr1-Ercc1^{ko/loxP}* mice microglia 5 days after tamoxifen treatment, indicating that 5 days of *Ercc1* deficiency was not sufficient to affect microglia gene expression (Figure 6b).

The number of differentially expressed genes, both up- and down-regulated, in microglia at different times after tamoxifen treatment, and associated GO terms are depicted in Figure 6d. The gene lists and enriched GO terms are provided in Table S4.

Microglia-specific deletion of *Ercc1* resulted in a gene expression signature distinct from the priming signature of aged and disease-associated microglia we previously reported (Holtman et al., 2015). Only 19 of the 458 genes upregulated at 2 months after tamoxifen treatment in *Cx3cr1-Ercc1^{ko/loxP}* microglia overlapped with this priming gene expression module consisting of 295 upregulated genes, suggesting microglia were not primed by intrinsic DNA damage repair deficiency (Figure 6e).

4 | DISCUSSION

Here, we analyzed the effect of *Ercc1*-deficiency on microglia. Deletion of *Ercc1* resulted in progressive microglia loss and to compensate

for this cell loss, microglia proliferation was transiently increased. Interestingly, the remaining *Ercc1*-deficient and nondeficient microglia both displayed increased proliferation activity. Gradually, likely due to ongoing loss of *Ercc1*-deficient microglia, the CNS gradually repopulated with nondeficient (*Ercc1^{ko/loxP}*) microglia. Unlike constitutive *Ercc1*-knockout mice, intrinsic *Ercc1* deletion did not induce microglia activation or priming. Microglia-specific deletion of *Ercc1* transiently induced an aging-associated gene expression profile, which was different from the gene expression signature of aged and CNS disease-associated microglia (Holtman et al., 2015).

4.1 | Phenotypes of microglia in conditional *Cx3cr1-Ercc1^{ko/loxP}* mice compared to constitutive *Ercc1^{Δ/ko}* mice

In constitutive *Ercc1^{Δ/ko}* mice, *Ercc1*-deficiency was already present in the zygote, and in all cell types. However, in *Cx3cr1-Ercc1^{ko/loxP}* mice, *Ercc1*-deficiency in *Cx3cr1*-expressing cells was induced by tamoxifen treatment in young adult mice (6–8 weeks of age). In constitutive *Ercc1^{Δ/ko}* mice, microglia density was increased but in *Cx3cr1-Ercc1^{ko/loxP}* mice, microglia were lost after *Ercc1* deletion. Constitutive *Ercc1* deletion resulted in a microglia priming gene expression signature (Holtman et al., 2015). In a previous study, we showed that *Camk2^{creER}*-driven *Ercc1* deletion in forebrain neurons also resulted in a microglia phenotype reminiscent of what was observed in *Ercc1^{Δ/ko}* mice (Raj et al., 2014). In contrast, although microglia from *Cx3cr1-Ercc1^{ko/loxP}* mice transiently displayed an aging gene expression profile at 2 months after tamoxifen treatment, no clear gene expression signature of priming was detected. Together, these results suggest that microglia priming can be triggered by neuronal genotoxic stress (Raj et al., 2014), but not by microglia-intrinsic genotoxic stress after *Ercc1* deletion. Nonetheless, *Ercc1* is an essential protein for microglia, as microglia deficient for *Ercc1* are progressively replaced by microglia with a functional *Ercc1* allele.

4.2 | Turnover of microglia in *Cx3cr1-Ercc1^{ko/loxP}* mice after tamoxifen treatment

Using genetic labeling and long-term in vivo imaging, Fügler et al. reported a median lifetime of mouse neocortical microglia of

FIGURE 6 Gene expression profile of microglia after *Ercc1* deletion. (a) Outline of microglia sampling. Microglia were isolated from *Cx3cr1-Ercc1^{wt/loxP}* and *Cx3cr1-Ercc1^{ko/loxP}* mice before and 5 days to 12 months after tamoxifen treatment. The gene profiles were generated by 3' QuantSeq. *Cx3cr1-Ercc1^{ko/loxP}* mice microglia without tamoxifen treatment served as nontamoxifen controls. (b) Heatmap of 1,670 differentially expressed genes through pairwise comparisons as described in Figure S4 (FDR < 0.05 and fold change > 1.5). These genes clustered into 7 groups. (c) GO analysis of different clusters. The genes in Clusters 2 and 3 were combined for GO analysis. The top 20 GO terms are shown. (d) The number of differentially up- and down-regulated genes between the indicated comparisons and associated GO terms are depicted (FDR < 0.05 and fold change > 1.5). (e) Venn diagram showing unique and overlapping genes and associated GO terms between 458 upregulated genes (*ko 2m tam* vs. *-tam* microglia) and priming signature of aged and disease-associated microglia (Holtman et al., 2015). The full lists of genes and enriched GO terms above mentioned are available in Table S4. *ctrl*, *Cx3cr1-Ercc1^{wt/loxP}* mice after tamoxifen treatment; *ko*, *Cx3cr1-Ercc1^{ko/loxP}* mice after tamoxifen treatment; *-tam*, *Cx3cr1-Ercc1^{ko/loxP}* mice without tamoxifen treatment

15 months (Füger et al., 2017). In a similar study, the turnover time of mouse microglia was estimated to be 41, 15, and 8 months in the cortex, hippocampus, and olfactory bulb, respectively (Tay et al., 2017). Askew et al. showed that 0.69% of the microglia population is proliferating with an estimated turnover time of 96 days (Askew et al., 2017). Despite these differences in reported turnover times, microglia are relatively long-lived cells in the CNS. Strikingly, after experimental depletion of microglia by either using mice expressing a CD11b-TK transgene (Gowing, Vallières, & Julien, 2006), CSF1R inhibitors (Rice et al., 2017), or the *Cx3cr1^{creER};iDTR* system, remaining microglia repopulated the CNS very fast (Bruttger et al., 2015; Elmore et al., 2014; Rubino et al., 2018; Varvel et al., 2012). The disadvantage of these approaches is the very fast depletion and repopulation, resulting in (transient) astrogliosis. And the repopulated microglia in the *Cx3cr1^{creER};iDTR* system have an altered, interferon regulatory factor 7-driven activation phenotype (Rubino et al., 2018; Waisman, Ginhoux, Greter, & Bruttger, 2015).

In the *Cx3cr1-Ercc1^{ko/loxP}* mice used in this study, *Ercc1*-deficient microglia were gradually lost, which was associated with a transient increase in proliferation. Similarly, Varol et al. reported a progressive replacement of *Dicer*-deficient microglia in *Cx3cr1^{creER};Dicer^{ko/loxP}* mice after tamoxifen treatment. Importantly, they further showed that *Dicer*-deficiency could induce DNA damage in newborn microglia (Varol et al., 2017). Most likely, *Ercc1* deficiency resulted in microglia apoptosis, reflected by the increased expression of apoptosis-related genes in *Cx3cr1-Ercc1^{ko/loxP}* microglia at 1 and 2 months after tamoxifen treatment (Figure 6bc, Cluster 2 and 3). Importantly, this gradual replacement of microglia did not result in microgliosis.

After pharmacologic depletion by CSF1R inhibitors, the repopulated microglia are derived from the remaining microglia population without contribution from peripheral myeloid cells (Elmore et al., 2014; Huang et al., 2018; Zhan, Sohn, Zhou, Li, & Gan, 2019). For genetic microglia ablation using the *Cx3cr1^{creER};iDTR* system, Bruttger et al. also showed that microglia exclusively renew from the remaining cells (Bruttger et al., 2015). However, Lund et al. showed that the repopulated microglia originated from remaining CX3CR1⁺F4/80^oClec12a⁻ microglia and CX3CR1⁺F4/80^{hi}Clec12a⁺ microglia-like macrophages originated from Ly6C^{hi} monocytes (Lund et al., 2018). These monocyte-derived macrophages can acquire some key features of microglia but still are transcriptionally and functionally distinct from CNS resident microglia even 12 weeks after depletion (Lund et al., 2018). In our study, at 12 months after tamoxifen treatment, the repopulated microglia are transcriptionally similar to microglia from control mice, suggesting that the repopulated microglia in *Cx3cr1-Ercc1^{ko/loxP}* mice are most likely derived from microglia that escaped Cre recombination.

4.3 | Morphology of microglia after *Ercc1* deletion

Microglia are pleomorphic and can adapt to different environments. Ramified microglia are relatively quiescent and surveil the parenchyma, while microglia with a more amoeboid phenotype are more

migratory, phagocytic and immune activated (Kettenmann, Hanisch, Noda, & Verkhratsky, 2011). Microglia morphometrics revealed significant alterations in microglia morphology in *Cx3cr1-Ercc1^{ko/loxP}* mice after tamoxifen treatment. Further analysis revealed this was mainly due to changes in a subset of microglia. Interestingly, this subset of microglia consisted of both *Ercc1*-deficient and nondeficient microglia, since this subset was detected at both 2 months (when the majority of microglia is *Ercc1^{ko/rec}*; Figure 2) and 12 months (when the majority of microglia is *Ercc1^{ko/loxP}*; Figure 2) after tamoxifen treatment. This suggests that, in compensation for the cell loss, both *Ercc1*-deficient (*Ercc1^{ko/rec}*) and nondeficient (*Ercc1^{ko/loxP}*) microglia became larger in size and more extensively ramified, likely in order to surveil a larger parenchymal area. However, potential functional differences between these enlarged cells and homeostatic microglia are still unresolved.

4.4 | Spontaneous recombinase activity of CreER

In this study, we used *Cx3cr1^{creER}* mice to delete *Ercc1* in microglia. Microglia deficient for *Ercc1* were gradually lost and replaced by *Ercc1^{ko/loxP}* microglia. The transcriptional changes we determined at different time points after tamoxifen treatment were generated using all microglia isolated from mouse brain. As a consequence, the effects of *Ercc1*-deficiency on gene expression might be diluted by *Ercc1^{ko/loxP}* microglia that progressively populate the brain after tamoxifen treatment. In order to separate *Ercc1*-deficient *Ercc1^{ko/rec}* microglia and nondeficient *Ercc1^{ko/loxP}* microglia, we generated a *Cx3cr1^{creERT2};Ercc1^{ko/loxP};R26^{CAG-tdTomato}* mouse line. In these mice, *Ercc1^{ko/rec}* microglia would also express the tdTomato reporter, where *Ercc1^{ko/loxP}* microglia do not. This assumes that the excision of the floxed *Ercc1* and floxed stop cassette upstream of the tdTomato reporter gene are equally efficient. However, we found 70% of the microglia already expressed the tdTomato reporter prior to tamoxifen treatment (data not shown). This “leaky” Cre activity of the *Cx3cr1^{creER}* transgene was confirmed by other studies (Chappell-Maor et al., 2020; Fonseca et al., 2017). In addition, for our *Cx3cr1^{creERT2};Ercc1^{ko/loxP};R26^{CAG-tdTomato}* reporter mouse line, we observed that the spontaneous activity of Cre only affected the floxed stop cassette upstream of tdTomato, but not the floxed sequence of our target gene *Ercc1*. This is most likely due to the size of the floxed fragment of our target gene *Ercc1*, which is around 2.5 kb (Doig et al., 2006), which is longer than the 0.8 kb floxed stop cassette in the tdTomato reporter (Madisen et al., 2010). The different susceptibility of constructs in response to basal CreERT2 activity has also been shown in other studies (Alvarez-Aznar et al., 2020; Van Hove et al., 2020). This tamoxifen-independent Cre activity made it impossible to distinguish between *Ercc1*-deficient and nondeficient microglia in our *Cx3cr1^{creERT2};Ercc1^{ko/loxP};R26^{CAG-tdTomato}* mice.

In summary, our data indicate that *Ercc1* is an essential protein for microglia and its deletion leads to cell death. As a consequence, microglia are gradually replaced by nondeficient *Ercc1^{ko/loxP}* microglia carrying a functional *Ercc1^{loxP}* allele. The replacement of *Ercc1*-deficient microglia by nondeficient microglia is not accompanied by



extensive immune activation or gliosis in the CNS. These data furthermore indicate that the functionality and gene expression changes observed in constitutive *Erc1^{Δ/ko}* mice are not microglia intrinsic but likely caused by an aging environment, in agreement with earlier postulations (Raj et al., 2014).

ACKNOWLEDGMENTS

The authors thank Amanda Sierra, Achucarro Basque Center for Neuroscience, Zamudio, Department of Neurosciences, University of the Basque Country EHU/UPV, Leioa, Spain for microscopic images. The authors thank Marloes Roorda, Tanja Grabietz, Qiong Jiang, and Ietje Mantingh-Otter for technical support. The authors thank Geert Mesander, Johan Teunis, Theo Bijma, Wayel Abdulahad, and Henk Moes of the UMCG FACS facility. This work was supported by China Scholarship Council fellowships to Xiaoming Zhang and Yang Heng.

DATA AVAILABILITY STATEMENT

The data that supports the findings of this study are available in the supplementary material of this article

ORCID

Susanne M. Kooistra <https://orcid.org/0000-0003-0211-8283>

Erik W. G. M. Boddeke <https://orcid.org/0000-0002-5058-9648>

Bart J. L. Eggen <https://orcid.org/0000-0001-8941-0353>

REFERENCES

- Ahmad, A., Robinson, A. R., Duensing, A., van Drunen, E., Beverloo, H. B., Weisberg, D. B., ... Niedernhofer, L. J. (2008). ERCC1-XPF endonuclease facilitates DNA double-strand break repair. *Molecular and Cellular Biology*, 28(16), 5082–5092.
- Alvarez-Aznar, A., Martinez-Corral, I., Daubel, N., Betsholtz, C., Makinen, T., & Gaengel, K. (2020). Tamoxifen-independent recombination of reporter genes limits lineage tracing and mosaic analysis using CreER(T2) lines. *Transgenic Research*, 29(1), 53–68.
- Askew, K., Li, K., Olmos-Alonso, A., Garcia-Moreno, F., Liang, Y., Richardson, P., ... Gomez-Nicola, D. (2017). Coupled proliferation and apoptosis maintain the rapid turnover of microglia in the adult brain. *Cell Reports*, 18(2), 391–405.
- Borgesius, N. Z., de Waard, M. C., van der Pluijm, I., Omrani, A., Zondag, G. C., van der Horst, G. T., ... Elgersma, Y. (2011). Accelerated age-related cognitive decline and neurodegeneration, caused by deficient DNA repair. *The Journal of Neuroscience*, 31(35), 12543–12553.
- Bruttger, J., Karram, K., Wortge, S., Regen, T., Marini, F., Hoppmann, N., ... Waisman, A. (2015). Genetic cell ablation reveals clusters of local self-renewing microglia in the mammalian central nervous system. *Immunity*, 43(1), 92–106.
- Butovsky, O., & Weiner, H. L. (2018). Microglial signatures and their role in health and disease. *Nature Reviews Neuroscience*, 19(10), 622–635.
- Chappell-Maor, L., Kolesnikov, M., Kim, J. S., Shemer, A., Haimon, Z., Grozovski, J., ... Jung, S. (2020). Comparative analysis of CreER transgenic mice for the study of brain macrophages: A case study. *European Journal of Immunology*, 50(3), 353–362.
- Cunningham, C. (2013). Microglia and neurodegeneration: The role of systemic inflammation. *Glia*, 61(1), 71–90.
- de Waard, M. C., van der Pluijm, I., Zuiderveen Borgesius, N., Comley, L. H., Haasdijk, E. D., Rijkse, Y., ... Jaarsma, D. (2010). Age-related motor neuron degeneration in DNA repair-deficient *Erc1* mice. *Acta Neuropathologica*, 120(4), 461–475.
- Doig, J., Anderson, C., Lawrence, N. J., Selfridge, J., Brownstein, D. G., & Melton, D. W. (2006). Mice with skin-specific DNA repair gene (*Erc1*) inactivation are hypersensitive to ultraviolet irradiation-induced skin cancer and show more rapid actinic progression. *Oncogene*, 25(47), 6229–6238.
- Dolle, M. E., Kuiper, R. V., Roodbergen, M., Robinson, J., de Vlugt, S., Wijnhoven, S. W., ... van Steeg, H. (2011). Broad segmental progeroid changes in short-lived *Erc1(-/Delta7)* mice. *Pathobiology of Aging & Age-related Diseases*, 1(1), 7219.
- Elmore, M. R., Najafi, A. R., Koike, M. A., Dagher, N. N., Spangenberg, E. E., Rice, R. A., ... Green, K. N. (2014). Colony-stimulating factor 1 receptor signaling is necessary for microglia viability, unmasking a microglia progenitor cell in the adult brain. *Neuron*, 82(2), 380–397.
- Fonseca, M. I., Chu, S. H., Hernandez, M. X., Fang, M. J., Modarresi, L., Selvan, P., ... Tenner, A. J. (2017). Cell-specific deletion of *C1qa* identifies microglia as the dominant source of *C1q* in mouse brain. *Journal of Neuroinflammation*, 14(1), 48.
- Füger, P., Hefendehl, J. K., Veeraraghavalu, K., Wendeln, A. C., Schlosser, C., Obermüller, U., ... Jucker, M. (2017). Microglia turnover with aging and in an Alzheimer's model via long-term in vivo single-cell imaging. *Nature Neuroscience*, 20(10), 1371–1376.
- Geirsdóttir, L., David, E., Keren-Shaul, H., Weiner, A., Bohlen, S. C., Neuber, J., ... Prinz, M. (2019). Cross-species single-cell analysis reveals divergence of the primate microglia program. *Cell*, 179(7), 1609–1622.
- Gerrits, E., Heng, Y., Boddeke, E., & Eggen, B. J. L. (2020). Transcriptional profiling of microglia; current state of the art and future perspectives. *Glia*, 68(4), 740–755.
- Gowing, G., Vallières, L., & Julien, J.-P. (2006). Mouse model for ablation of proliferating microglia in acute CNS injuries. *Glia*, 53(3), 331–337.
- Gregg, S. Q., Robinson, A. R., & Niedernhofer, L. J. (2011). Physiological consequences of defects in ERCC1-XPF DNA repair endonuclease. *DNA Repair*, 10(7), 781–791.
- Heng, Y., Eggen, B. J. L., Boddeke, E. W. G. M., & Kooistra, S. M. (2017). Mouse models of central nervous system ageing. *Drug Discovery Today: Disease Models*, 25–26, 21–34.
- Holtman, I. R., Raj, D. D., Miller, J. A., Schaafsma, W., Yin, Z., Brouwer, N., ... Eggen, B. J. (2015). Induction of a common microglia gene expression signature by aging and neurodegenerative conditions: A co-expression meta-analysis. *Acta Neuropathologica Communications*, 3(1), 31.
- Huang, Y., Xu, Z., Xiong, S., Sun, F., Qin, G., Hu, G., ... Peng, B. (2018). Repopulated microglia are solely derived from the proliferation of residual microglia after acute depletion. *Nature Neuroscience*, 21(4), 530–540.
- Kashiyama, K., Nakazawa, Y., Pilz, D. T., Guo, C., Shimada, M., Sasaki, K., ... Ogi, T. (2013). Malfunction of nuclease ERCC1-XPF results in diverse clinical manifestations and causes Cockayne syndrome, Xeroderma Pigmentosum, and Fanconi Anemia. *The American Journal of Human Genetics*, 92(5), 807–819.
- Keren-Shaul, H., Spinrad, A., Weiner, A., Matcovitch-Natan, O., Dvir-Szternfeld, R., Ulland, T. K., ... Toth, B. (2017). A unique microglia type associated with restricting development of Alzheimer's disease. *Cell*, 169, 1276–1290.e17.
- Kettenmann, H., Hanisch, U. K., Noda, M., & Verkhratsky, A. (2011). Physiology of microglia. *Physiological Reviews*, 91(2), 461–553.
- Klein Douwel, D., Boonen, R. A., Long, D. T., Szypowska, A. A., Raschle, M., Walter, J. C., & Knipscheer, P. (2014). XPF-ERCC1 acts in unhooking DNA interstrand crosslinks in cooperation with FANCD2 and FANCP/SLX4. *Molecular Cell*, 54(3), 460–471.
- Krasemann, S., Madore, C., Cialic, R., Baufeld, C., Calcagno, N., El Fatimy, R., ... Butovsky, O. (2017). The TREM2-APOE pathway drives the transcriptional phenotype of dysfunctional microglia in neurodegenerative diseases. *Immunity*, 47(3), 566–581 e569.
- Le May, N., Mota-Fernandes, D., Velez-Cruz, R., Iltis, I., Biard, D., & Egly, J. M. (2010). NER factors are recruited to active promoters and

- facilitate chromatin modification for transcription in the absence of exogenous genotoxic attack. *Molecular Cell*, 38(1), 54–66.
- Li, S., Lu, H., Wang, Z., Hu, Q., Wang, H., Xiang, R., ... Wu, X. (2019). ERCC1/XPF is important for repair of DNA double-Strand breaks containing secondary structures. *iScience*, 16, 63–78.
- Livak, K. J., & Schmittgen, T. D. (2001). Analysis of relative gene expression data using real-time quantitative PCR and the 2⁻ΔΔCT method. *Methods*, 25(4), 402–408.
- Lund, H., Pieber, M., Parsa, R., Han, J., Grommisch, D., Ewing, E., ... Harris, R. A. (2018). Competitive repopulation of an empty microglial niche yields functionally distinct subsets of microglia-like cells. *Nature Communications*, 9(1), 4845.
- Madisen, L., Zwingman, T. A., Sunkin, S. M., Oh, S. W., Zariwala, H. A., Gu, H., ... Zeng, H. (2010). A robust and high-throughput Cre reporting and characterization system for the whole mouse brain. *Nature Neuroscience*, 13(1), 133–140.
- Mathys, H., Adaiikkan, C., Gao, F., Young, J. Z., Manet, E., Hemberg, M., ... Tsai, L. H. (2017). Temporal tracking of microglia activation in neurodegeneration at single-cell resolution. *Cell Reports*, 21(2), 366–380.
- McDonough, A., Noor, S., Lee, R. V., Dodge, R., Strosnider, J. S., Shen, J., ... Weinstein, J. R. (2020). Ischemic preconditioning induces cortical microglial proliferation and a transcriptomic program of robust cell cycle activation. *Glia*, 68(1), 76–94.
- McKinnon, P. J. (2013). Maintaining genome stability in the nervous system. *Nature Neuroscience*, 16(11), 1523–1529.
- Norbury, C. J., & Zhivotovsky, B. (2004). DNA damage-induced apoptosis. *Oncogene*, 23(16), 2797–2808.
- Parkhurst, C. N., Yang, G., Ninan, I., Savas, J. N., Yates, J. R., 3rd, Lafaille, J. J., ... Gan, W. B. (2013). Microglia promote learning-dependent synapse formation through brain-derived neurotrophic factor. *Cell*, 155(7), 1596–1609.
- Raj, D. D., Jaarsma, D., Holtman, I. R., Olah, M., Ferreira, F. M., Schaafsma, W., ... Boddeke, H. W. (2014). Priming of microglia in a DNA-repair deficient model of accelerated aging. *Neurobiology of Aging*, 35(9), 2147–2160.
- Rice, R. A., Pham, J., Lee, R. J., Najafi, A. R., West, B. L., & Green, K. N. (2017). Microglial repopulation resolves inflammation and promotes brain recovery after injury. *Glia*, 65(6), 931–944.
- Rodier, F., Coppe, J. P., Patil, C. K., Hoeijmakers, W. A., Munoz, D. P., Raza, S. R., ... Campisi, J. (2009). Persistent DNA damage signalling triggers senescence-associated inflammatory cytokine secretion. *Nature Cell Biology*, 11(8), 973–979.
- Rubino, S. J., Mayo, L., Wimmer, I., Siedler, V., Brunner, F., Hametner, S., ... Weiner, H. L. (2018). Acute microglia ablation induces neurodegeneration in the somatosensory system. *Nature Communications*, 9(1), 4578.
- Schumacher, B., Garinis, G. A., & Hoeijmakers, J. H. (2008). Age to survive: DNA damage and aging. *Trends in Genetics*, 24(2), 77–85.
- Stoppini, L., Buchs, P. A., & Muller, D. (1991). A simple method for organotypic cultures of nervous tissue. *Journal of Neuroscience Methods*, 37(2), 173–182.
- Tay, T. L., Mai, D., Dautzenberg, J., Fernandez-Klett, F., Lin, G., Sagar, ... Prinz, M. (2017). A new fate mapping system reveals context-dependent random or clonal expansion of microglia. *Nature Neuroscience*, 20(6), 793–803.
- Van Hove, H., Antunes, A. R. P., De Vlaminck, K., Scheyltjens, I., Van Ginderachter, J. A., & Movahedi, K. (2020). Identifying the variables that drive tamoxifen-independent CreERT2 recombination: Implications for microglial fate mapping and gene deletions. *European Journal of Immunology*, 50(3), 459–463.
- Varol, D., Mildner, A., Blank, T., Shemer, A., Barashi, N., Yona, S., ... Jung, S. (2017). Dicer deficiency differentially impacts microglia of the developing and adult brain. *Immunity*, 46(6), 1030–1044.
- Varvel, N. H., Grathwohl, S. A., Baumann, F., Liebig, C., Bosch, A., Brawek, B., ... Jucker, M. (2012). Microglial repopulation model reveals a robust homeostatic process for replacing CNS myeloid cells. *Proceedings of the National Academy of Sciences of the United States of America*, 109(44), 18150–18155.
- Vegh, M. J., de Waard, M. C., van der Pluijm, I., Ridwan, Y., Sassen, M. J., van Nierop, P., ... van Kesteren, R. E. (2012). Synaptic proteome changes in a DNA repair deficient ercc1 mouse model of accelerated aging. *Journal of Proteome Research*, 11(3), 1855–1867.
- Waisman, A., Ginhoux, F., Greter, M., & Bruttger, J. (2015). Homeostasis of microglia in the adult brain: Review of novel microglia depletion systems. *Trends in Immunology*, 36(10), 625–636.
- Weeda, G., Donker, I., de Wit, J., Morreau, H., Janssens, R., Vissers, C. J., ... Hoeijmakers, J. H. (1997). Disruption of mouse ERCC1 results in a novel repair syndrome with growth failure, nuclear abnormalities and senescence. *Current Biology*, 7(6), 427–439.
- Zhan, L., Sohn, P. D., Zhou, Y., Li, Y., & Gan, L. (2019). A Mac2-positive progenitor-like microglial population survives independent of CSF1R signaling in adult mouse brain. *bioRxiv*, 722090.

SUPPORTING INFORMATION

Additional supporting information may be found online in the Supporting Information section at the end of this article.

How to cite this article: Zhang X, Heng Y, Kooistra SM, et al. Intrinsic DNA damage repair deficiency results in progressive microglia loss and replacement. *Glia*. 2021;69:729–745. <https://doi.org/10.1002/glia.23925>